Coherent quadrupole-octupole modes and split parity-doublet spectra in odd-*A* nuclei

N. Minkov, S. Drenska, and P. Yotov
Institute of Nuclear Research and Nuclear Energy, Bulgarian Academy of Sciences, Tzarigrad Road 72, BG-1784 Sofia, Bulgaria

S. Lalkovski
Department of Physics, University of Sofia, 1164 Sofia, Bulgaria and
School of Engineering, University of Brighton, Brighton BN2 4GJ, United Kingdom

D. Bonatsos
Institute of Nuclear Physics, N.C.S.R. "Demokritos" GR-15310 Aghia Paraskevi, Attiki, Greece

W. Scheid
Institut für Theoretische Physik der Justus-Liebig-Universität, Heinrich-Buff-Ring 16, D-35392 Giessen, Germany
(Received 26 March 2007; revised manuscript received 21 May 2007; published 26 September 2007)

A collective model describing coherent quadrupole-octupole oscillations and rotations with a Coriolis coupling between the even-even core and the unpaired nucleon is applied to odd nuclei. The particle-core coupling provides a parity-doublet structure of the spectrum, whereas the quadrupole-octupole motion leads to a splitting of the doublet energy levels. The formalism successfully reproduces the split parity-doublet spectra and the attendant $B(E1)$ and $B(E2)$ transition probabilities in a wide range of odd-A nuclei. It provides estimations for the influence of the Coriolis interaction on the collective motion and subsequently for the value of angular momentum projection K on which the spectrum is built. The analysis of the energy splitting and $B(E1)$ transition probabilities between opposite parity counterparts suggests degenerate doublet structures at high angular momenta. The study provides information about the evolution of quadrupole-octupole collectivity in odd-mass nuclei.

DOI: 10.1103/PhysRevC.76.034324 PACS number(s): 21.60.Ev, 21.10.Re

I. INTRODUCTION

The simultaneous manifestation of quadrupole and octupole degrees of freedom in atomic nuclei is associated with typical spectroscopic characteristics of nuclear collective motion [1]. In general the spectrum contains positive- and negative-parity levels, some of them related with enhanced electric $E1$ and $E3$ transitions [2]. In even-even nuclei the even and odd angular momentum levels appear with positive and negative parities, respectively, due to the shape reflection asymmetry [3–6]. In the regions of pronounced quadrupole-octupole deformations, e.g., in the region of light actinide nuclei, the alternating parity levels form a single octupole band, whereas in nuclei toward transition and nearly vibration regions both positive- and negative-parity sequences remain essentially separated from each other. In odd nuclei the structure of the spectrum is determined by the coupling between the reflection asymmetric even-even core and the motion of the unpaired particle. The combination of the intrinsic parity of core with that of the particle to a "total intrinsic parity" provides a split-parity doublet structure of the spectrum. The mutual disposition of the doublet counterparts up or down depends on the parity of the ground state as well as on the possible change in the intrinsic parity at some higher angular momenta. As in some cases, especially in heavy odd nuclei, the angular momentum of the ground state and/or its projection K are not unambiguously determined, the complicated structure of the spectrum represents a challenging subject for a study from both experimental and theoretical points of view.

In the above aspect various theoretical models, developed initially to explain the properties of quadrupole-octupole deformations in even-even nuclei, have been extended to describe the respective properties in odd nuclei [2,7,8]. Recently a collective model for the quadrupole-octupole vibration and rotation motion of even-even nuclei has been proposed [9]. It was able to reproduce basic characteristics such as energy levels, parity shift, and electric transition properties in nuclei with collective bands built on coherent quadrupole-octupole vibrations.

The purpose of the present work is to extend the coherent quadrupole-octupole model approach [9] to the case of odd nuclei and to apply it to collective spectra in the region of heavy odd nuclei. For this reason we consider the Coriolis coupling of the "soft" quadrupole-octupole oscillating core to the motion of the unpaired nucleon. The model scheme is developed, respectively, to take into account the total intrinsic parity of the system and to incorporate consequently the split-parity doublet structure of the spectrum.

As it is shown below such a formalism allows one not only to reproduce the energy levels and electromagnetic transition characteristics of parity doublet spectra but also to examine the behavior of the parity splitting in dependence on the angular momentum. Within this framework it is possible to study the effects of the Coriolis coupling on the fine structure of the spectrum. It is also possible to estimate the respective values of the angular momentum projection K and subsequently the related single-particle configurations dominating the intrinsic nuclear structure.

From another point of view the proposed approach can be used to study the changes in the structure of parity-doublet spectra in different nuclear regions and subsequently

the evolution of the quadrupole-octupole collectivity in odd nuclei. As it will be illustrated below the concept of a coherent quadrupole-octupole motion is supported by data from quite a large number of odd-A nuclei. Moreover, the regions where split-parity doublet spectra are formed appear to be experimentally better developed than the corresponding regions in even-even nuclei where alternating parity spectra are observed. This circumstance determines the need to examine the limits of manifestation of quadrupole-octupole collectivity in odd-A nuclei. Analysis in this direction is of interest from both collective and intrinsic (microscopic) points of view.

The article is organized as follows. In Sec. II the quadrupole-octupole Hamiltonian with the Coriolis interaction is presented. The model mechanism for the appearance of split-parity doublet spectra is explained in Sec. III. The model expressions for reduced $B(E1)$, $B(E2)$, and $B(E3)$ transitions in these spectra are given in Sec. IV. Numerical results and discussion on the application of the model in various nuclear regions are given in Sec. V. Section VI contains some concluding remarks.

II. QUADRUPOLE-OCTUPOLE HAMILTONIAN WITH CORIOLIS INTERACTION

We consider that the even-even core of an odd nucleus can oscillate with respect to the quadrupole (β_2) and octupole (β_3) axial deformation variables mixed through a centrifugal (rotation-vibration) interaction. The unpaired nucleon couples to the collective motion through the Coriolis interaction. The collective Hamiltonian of the odd nucleus can then be taken in the form

$$H_{\rm qo} = -\frac{\hbar^2}{2B_2}\frac{\partial^2}{\partial\beta_2^2} - \frac{\hbar^2}{2B_3}\frac{\partial^2}{\partial\beta_3^2} + U(\beta_2,\beta_3,I) + H_{\rm coriol}, \quad (1)$$

where

$$U(\beta_2,\beta_3,I) = \frac{1}{2}C_2{\beta_2}^2 + \frac{1}{2}C_3{\beta_3}^2 + \frac{\hat{I}^2 - \hat{I}_z^2}{2\left(d_2\beta_2^2 + d_3\beta_3^2\right)} \quad (2)$$

is the potential of the quadrupole and octupole oscillations coupled through the collective angular momentum $\hat{I}$ and its third projection $\hat{I}_z$. B_2 and B_3 are the effective quadrupole and octupole mass parameters and C_2 and C_3 are the stiffness parameters for the respective oscillation modes. The last term in Eq. (1) represents the Coriolis interaction, which is set

$$H_{\rm coriol} = -\frac{(\hat{I}_+\hat{j}_- + \hat{I}_-\hat{j}_+)}{2\left(d_2\beta_2^2 + d_3\beta_3^2\right)}. \quad (3)$$

Here, $\hat{I}_\pm = \hat{I}_x \pm i\hat{I}_y$ and $\hat{j}_\pm = \hat{j}_x \pm i\hat{j}_y$ are the spherical components of the total nuclear and the intrinsic (unpaired) particle angular momenta, respectively. The quantity $\mathcal{L}^{(\rm quad+oct)} = (d_2\beta_2^2 + d_3\beta_3^2)$ can be associated to the moment of inertia of an axially symmetric quadrupole-octupole deformed shape [10].

After taking into account the action of the total angular momentum operators and the Coriolis term in the "particle+rotor" space, Eq. (3) can be superposed to the third term in Eq. (2). Then the terms $U(\beta_2,\beta_3,I)$ and $H_{\rm coriol}$ in Eq. (1) are replaced by the potential

$$U(\beta_2,\beta_3,I,K,\pi a) = \frac{1}{2}C_2\beta_2^2 + \frac{1}{2}C_3\beta_3^2 + \frac{X(I,K,\pi a)}{d_2\beta_2^2 + d_3\beta_3^2}, \quad (4)$$

where

$$X(I,K,\pi a) = \frac{1}{2}\left[d_0 + I(I+1) - K^2 + \pi a\delta_{K,\frac{1}{2}}(-1)^{I+1/2}\left(I+\frac{1}{2}\right)\right]. \quad (5)$$

The decoupling parameter a is defined between the unpaired particle states $a = \langle\chi_K|\hat{j}_+|\chi_{-K}\rangle$ (with $K = 1/2$). The sign of its contribution in the potential energy depends on the total intrinsic parity $\pi = \pm$ of the system (see below). The parameter d_0 is introduced additionally to characterize the shape of the potential in the ground state.

The properties of the even core potential (2) have been studied in detail in Ref. [9]. We remark that the total "core+particle" potential (4) carries the same dependence on the variables β_2 and β_3, and on the collective angular momentum I. That is why in the following we recall only the main properties of the system based on this potential and present the basic items in the underlying eigenvalue/eigenstate problem.

In Ref. [9] it has been shown that if a condition for the simultaneous presence of nonzero coordinates ($\beta_{2\rm min}$, $\beta_{3\rm min}$) of the potential minimum is imposed, the stiffness and inertial parameters of the system are correlated as

$$\frac{d_2}{C_2} = \frac{d_3}{C_3}. \quad (6)$$

In this case the potential bottom represents an ellipse in the space of β_2 and β_3 that surrounds the infinite zero-deformation core. If prolate quadrupole deformations $\beta_2 > 0$ are considered, the system is characterized by oscillations between positive and negative β_3 values along the ellipse surrounding the potential core. Then it is convenient to use polar variables

$$\beta_2 = \frac{\eta}{\sqrt{d_2/d}}\cos\phi; \quad \beta_3 = \frac{\eta}{\sqrt{d_3/d}}\sin\phi \quad (7)$$

with $d = (d_2 + d_3)/2$. Under the condition (6), the potential energy depends only on the new deformation variable η and on the angular momentum I, and not on the angular variable ϕ. Then the transformed potential reads

$$U_{I,K,\pi a}(\eta) = \frac{1}{2}C\eta^2 + \frac{X(I,K,\pi a)}{d\eta^2} \quad (8)$$

where C is defined according to Eq. (6) as $1/C = d_2/(dC_2) = d_3/dC_3$. Further, by assuming that the quadrupole and octupole modes are represented in the collective motion with the same oscillation frequencies, one has the following relation between the quadrupole and octupole mass and inertia parameters:

$$\frac{d_2}{dB_2} = \frac{d_3}{dB_3} = \frac{1}{B}. \quad (9)$$

The above assumption corresponds to a coherent quadrupole-octupole motion of the system. As a result the model

Hamiltonian obtains a simple form in the polar variables

$$H_{qo} = -\frac{\hbar^2}{2B}\left(\frac{\partial^2}{\partial\eta^2} + \frac{1}{\eta}\frac{\partial}{\partial\eta} + \frac{1}{\eta^2}\frac{\partial^2}{\partial\phi^2}\right) + U_{I,K,\pi a}(\eta). \quad (10)$$

The quadrupole-octupole oscillation wave function can be taken in a separable form $\Phi(\eta,\phi) = \psi(\eta)\varphi(\phi)$. Then the Schrödinger equation for the Hamiltonian (10) with the potential (8) leads to the following separate equations for the variables η and ϕ

$$\frac{\partial^2}{\partial\eta^2}\psi(\eta) + \frac{1}{\eta}\frac{\partial}{\partial\eta}\psi(\eta) + \frac{2B}{\hbar^2}\left[E - \frac{\hbar^2}{2B}\frac{k^2}{\eta^2} - U_{I,K,\pi a}(\eta)\right]\psi(\eta) = 0; \quad (11)$$

$$\frac{\partial^2}{\partial\phi^2}\varphi(\phi) + k^2\varphi(\phi) = 0, \quad (12)$$

where k is the separation quantum number. Equation (11) with the potential (8) is similar to the equation for the Davidson potential [11], which is analytically solvable [12,13]. Thus Eq. (11) is solved analytically providing the following explicit expression for the energy spectrum

$$E_{n,k}(I,K,\pi a) = \hbar\omega[2n + 1 + \sqrt{k^2 + bX(I,K,\pi a)}], \quad (13)$$

where $\omega = \sqrt{C/B}$, $n = 0, 1, 2, \ldots$ and $b = 2B/(\hbar^2 d)$. The respective eigenfunctions $\psi(\eta)$ are obtained in terms of the Laguerre polynomials

$$\psi_n^I(\eta) = \sqrt{\frac{2\Gamma(n+1)}{\Gamma(n+2s+1)}}e^{-c\eta^2/2}(c\eta^2)^s L_n^{2s}(c\eta^2), \quad (14)$$

where $c = \sqrt{BC}/\hbar$ and $s = (1/2)\sqrt{k^2 + bX(I,K,\pi a)}$.

Equation (12) in the variable ϕ is solved under the boundary condition $\varphi(-\pi/2) = \varphi(\pi/2) = 0$, which provides two different solutions with positive and negative parities, $\pi_\varphi = (+)$ and $\pi_\varphi = (-)$, respectively

$$\varphi^+(\phi) = \sqrt{2/\pi}\cos(k\phi), \quad k = 1, 3, 5, \ldots; \quad (15)$$

$$\varphi^-(\phi) = \sqrt{2/\pi}\sin(k\phi), \quad k = 2, 4, 6, \ldots. \quad (16)$$

If the lowest energy of the motion in the variable ϕ is considered, one has $k = k_+ = 1$ for φ^+ and $k = k_- = 2$ for φ^-. The total wave function of the core+particle system has the form

$$\Psi^\pi_{nIMK}(\eta,\phi) = \psi_n^I(\eta)\varphi^\pm(\phi)\sqrt{\frac{2I+1}{16\pi^2}}\left[D^I_{KM}(\theta)\chi_K \pm (-1)^{I+K}D^I_{-KM}(\theta)\chi_{-K}\right]. \quad (17)$$

The total intrinsic parity π is determined as

$$\pi = \pi_\varphi \cdot \pi_\chi, \quad (18)$$

where π_φ is the parity of the even-core oscillation function $\varphi^\pm(\phi)$ and π_χ is the parity of the unpaired particle function χ_K.

TABLE I. Lowest values of the separation quantum number k, Eqs. (15) and (16), determined through Eq. (18) and the respective ways for the splitting of the parity doublet.

π_χ	I^π	π_φ	k	Shift
(+)	I^+	(+)	1	Down
	I^-	(−)	2	Up
(−)	I^+	(−)	2	Up
	I^-	(+)	1	Down

III. MODEL MECHANISM FOR THE SPLIT-PARITY DOUBLET SPECTRA

The coupling of the core and the unpaired nucleon in the core+particle system having the total wave function (17) provides a parity doublet structure of the spectrum

$$I^{(\pi=\pm)} = I_0^\pm, (I_0+1)^\pm, (I_0+2)^\pm, (I_0+3)^\pm, \ldots, \quad (19)$$

where I_0 is the angular momentum (half integer) of the ground state. The parity of the core oscillation wave function $\varphi^\pm(\phi)$ is determined by Eq. (18) as $\pi_\varphi = \pi \cdot \pi_\chi$. As a result the parity doublets are split with respect to the quantum number k in Eq. (13). The possible ways of splitting are shown in Table I.

It is seen that the direction in which the positive- and negative-parity counterparts of the doublet are shifted to each other depends on the parity of the unpaired-nucleon state. For the lowest energy part of the spectrum we may consider that the parity of the unpaired nucleon coincides with that of the ground state. Thus when the ground-state parity is positive, the negative counterparts of the doublet are shifted up with respect to the positive ones, whereas for a negative-parity ground state the opposite situation is realized. At some higher angular momentum the intrinsic nucleon parity can be changed due to an alignment process in the core [14]. Then the parity π_χ of the unpaired nucleon changes in sign. The parity π_φ of the core oscillation function also changes due to the relation (18). As a result the sign of the parity splitting of the states with $I^\pm$ is changed according to the scheme given in Table I. This effect can be easily identified in the structure of the experimental spectra. In the present model the change in the intrinsic nucleon parity at given angular momentum is taken into account phenomenologically by switching the selection rule for the quantum number k between the first ($\pi_\chi = +$) and the second ($\pi_\chi = -$) rows in Table I. This change can be taken into account microscopically through a consideration of the intrinsic single-particle structure within a deformed shell model [14].

Looking at Eq. (13) one can easily deduce that the relative displacement of the positive- and negative-parity counterparts in the spectrum decreases with the increasing angular momentum. At very high angular momenta the contribution of the quantum number k in the square root in Eq. (13) becomes negligible compared to the angular momentum term $bX(I,K,\pi a)$. As a result the split-parity spectrum gradually transforms to a degenerate parity doublet. In this way the model energy expression suggests that in the high spin region the total core+particle system is less affected by the parity of

the single-particle wave function. However, in regions where alignment processes take place, the sensitivity of the nucleus to the single-particle degrees of freedom becomes larger again, as discussed in the above paragraph.

IV. ELECTRIC TRANSITION PROBABILITIES IN THE SPLIT-PARITY DOUBLET SPECTRUM

The model formalism for $E1, E2$, and $E3$ transition probabilities in the system with coherent quadrupole-octupole motion is generally developed for even-even nuclei in Ref. [9]. Below we give the formulas modified for calculations of reduced transition probabilities in the split-parity doublets of odd-A nuclei by pointing out some particular characteristics related to the presence of a single particle.

The reduced probability for an electric transition with multipolarity $\lambda = 1, 2, 3$ between two states of the parity doublet characterized by the wave function (17) is

$$B\left(E\lambda; I_i^{\pi_i} \to I_f^{\pi_f}\right) = \frac{1}{2I_i+1} \sum_{M_i M_f \mu} \left|\left\langle \Psi^{\pi_f}_{n_f I_f M_f K_f}(\eta,\, \phi)\right|\right. \times \mathcal{M}_\mu(E\lambda)\left|\Psi^{\pi_i}_{n_i I_i M_i K_i}(\eta,\, \phi)\right\rangle\Big|^2, \quad (20)$$

where the transition operator $\mathcal{M}_\mu(E\lambda)$ is defined in terms of the variables η and ϕ as shown in Ref. [9]. Considering only the yrast parity-doublet spectrum with $n_i = n_f = 0$ and assuming that all states in the doublet are based on the same value of the angular momentum projection $K = K_i = K_f$, one has

$$B\left(E\lambda, I_i^{\pi_i} \to I_f^{\pi_f}\right) = b_\lambda \langle I_i K \lambda 0 | I_f K\rangle^2 S^2(E\lambda, I_i \to I_f)\left(\mathcal{I}^{\pi_\varphi^i \pi_\varphi^f}_{E\lambda}\right)^2, \quad (21)$$

where b_λ ($\lambda = 1, 2, 3$) are scaling constants related to effective charges, and

$$S(E1, I_i \to I_f) = \int_0^\infty d\eta \psi_0^{I_f}(\eta)\eta^3 \psi_0^{I_i}(\eta) = \frac{1}{c^2} \frac{\Gamma(s_i + s_f + 2)}{\sqrt{\Gamma(2s_i+1)\,\Gamma(2s_f+1)}} \quad (22)$$

$$S(E\lambda, I_i \to I_f) = \int_0^\infty d\eta \psi_0^{I_f}(\eta)\eta^2 \psi_0^{I_i}(\eta) = \frac{1}{c^{3/2}} \frac{\Gamma(s_i + s_f + \frac{3}{2})}{\sqrt{\Gamma(2s_i+1)\,\Gamma(2s_f+1)}}, \quad \lambda = 2, 3, \quad (23)$$

with

$$s_i = (1/2)\sqrt{k_i^2 + bX\left(I_i^{\pi_i}\right)}, \quad s_f = (1/2)\sqrt{k_f^2 + bX\left(I_f^{\pi_f}\right)}, \quad c = \sqrt{BC}/\hbar = \text{const}.$$

The integrals over the angular variable ϕ are

$$\mathcal{I}^{++}_{E2} = \frac{2}{\pi}\int_{-\pi/2}^{\pi/2} \cos^3\phi d\phi = \frac{8}{3\pi} \quad (24)$$

$$\mathcal{I}^{--}_{E2} = \frac{2}{\pi}\int_{-\pi/2}^{\pi/2} \cos\phi \sin^2(2\phi) d\phi = \frac{32}{15\pi} \quad (25)$$

$$\mathcal{I}^{+-}_{E1} = \frac{2}{\pi}\int_{-\pi/2}^{\pi/2} \cos^2\phi \sin\phi \sin(2\phi) d\phi = \frac{16}{15\pi} \quad (26)$$

$$\mathcal{I}^{+-}_{E3} = \frac{2}{\pi}\int_{-\pi/2}^{\pi/2} \cos\phi \sin\phi \sin(2\phi) d\phi = \frac{1}{2}. \quad (27)$$

We should remark that the above integrals (24)–(27), although being identical in form to integrals (42)–(45) of Ref. [9], enter in a different way the $B(E\lambda)$ expressions and more specifically the $B(E2)$ reduced probabilities in odd-A nuclei. Although the integrals I^{π_i,π_f} in Ref. [9] are determined by the total parities, the present integrals $\mathcal{I}^{\pi_\varphi^i \pi_\varphi^f}$ are determined by the parities of the quadrupole-octupole oscillation functions, which may not coincide with the total parities because of relation (18). As a result one has different contributions of the integrals (24)–(27) to the model $B(E2)$ values in dependence on the parity of the single particle function π_χ as follows, for $\pi_\chi = (+)$

$$B(E2; I_i^+ \to I_f^+) \sim \mathcal{I}^{++}_{E2} = 8/(3\pi) \quad (28)$$

$$B(E2; I_i^- \to I_f^-) \sim \mathcal{I}^{--}_{E2} = 32/(15\pi), \quad (29)$$

whereas in the opposite situation $\pi_\chi = (-)$

$$B(E2; I_i^+ \to I_f^+) \sim \mathcal{I}^{--}_{E2} = 32/(15\pi) \quad (30)$$

$$B(E2; I_i^- \to I_f^-) \sim \mathcal{I}^{++}_{E2} = 8/(3\pi). \quad (31)$$

Thus for $\pi_\chi = (+)$ the $B(E2)$ transition probabilities between positive-parity members of the doublet appear slightly enhanced with respect to the probabilities between the negative ones. For $\pi_\chi = (-)$ an enhancement in the $B(E2)$ transition probabilities between the negative-parity states is predicted. The model predictions for $B(E1)$ and $B(E3)$ transition probabilities between states with different parity do not show such a peculiarity since $\mathcal{I}^{+-}_{E\lambda} = \mathcal{I}^{-+}_{E\lambda}$.

V. NUMERICAL RESULTS AND DISCUSSION

The split-parity doublet structure of the spectrum is observed in a wide range of heavy odd nuclei, allowing a detailed test for the present coherent quadrupole-octupole model scheme. As a first step in this direction we examined various nuclear regions to identify possible parity-doublet structures. We have considered the presence of $E1$ transition intensities between positive- and negative-parity levels as a strong criterion for the forming of a parity-doublet structure based on quadrupole-octupole degrees of freedom. A weaker criterion based on the specific level ordering of positive- and negative-parity states was also applied to get more general systematic information about the evolution of quadrupole-octupole collectivity in odd-A nuclei.

In this framework, we applied the model to several nuclear regions obtaining a reasonable description of the respective experimental data. The applicability of the model scheme has been verified for the nuclei ^{151}Nd, ^{151,153}Pm, ^{153,155}Sm, $^{153-159}$Eu, ^{157,159}Gd, $^{157-163}$Tb, $^{159-165}$Dy, $^{163-169}$Ho, $^{219-225}$Fr, $^{219-227}$Ra, $^{219-227}$Ac, ^{223,225,229,231}Th, ^{233}Pa,

$^{233-237}$U, $^{235-239}$Np, $^{237-243}$Pu, $^{239-245}$Am, ^{245,247}Cm, and ^{247,249}Bk. The model descriptions were obtained by taking the theoretical energy levels $\tilde{E}_{0,k}(I) = E_{0,k}(I) - E_{0,k}(I_0)$ from Eq. (13), with I_0 being the ground-state angular momentum. The model parameters ω, b, d_0 and the decoupling parameter a (for the case of $K = 1/2$) have been adjusted with respect to the experimental data. In the cases where $B(E1)$ and/or $B(E2)$ transition probabilities are described, the available experimental data were fitted together with the energy values by adjusting the parameter c in Eqs. (22) and (23). The angular momentum projection K was taken as suggested in the experimental references, whereas for nuclei without suggestions we have assumed $K = I_0$. In all considered nuclei the calculations successfully reproduce the energy levels with both positive and negative parities.

Hereafter we give several representative examples for the model descriptions obtained in different regions of heavy nuclei. In Tables II and III the theoretical and the experimental levels of the nuclei ^{161,163}Dy, ^{219,221}Fr, ^{223,225}Th, ^{237}U, and ^{239}Pu are compared. The parameters of the fits are given also there. In the cases of gaps in the sequences of experimental data the calculations provide respective model predictions.

In Table II the results obtained for the nuclei ^{161}Dy and ^{163}Dy illustrate the applicability of the model in the rare earth region. These nuclei possess one of the best-developed parity-doublet structure among the odd-A rare-earth nuclei,

TABLE II. Theoretical and experimental energy levels (in keV) of the positive- and negative-parity bands in the nuclei ^{161,163}Dy, ^{219,221}Fr, and ^{223,225}Th. The values of ω are given in MeV/$\hbar$, whereas b and d_0 are in $\hbar^{-2}$ and $\hbar^2$, respectively. The Coriolis parameter a is in units $\hbar$, whereas c is dimensionless. The root-mean-square (RMS) deviations (in keV) are given in the first column. The data for ^{161}Dy, ^{219}Fr and ^{223}Th are taken from Ref. [15], whereas those for ^{163}Dy, ^{221}Fr and ^{225}Th are from Refs. [16,17] and [18], respectively.

Nucl./K params.	I	$\pi = (+)$		$\pi = (-)$		Nucl./K params.	I	$\pi = (+)$		$\pi = (-)$	
		Th.	Exp.	Th.	Exp.			Th.	Exp.	Th.	Exp.
^{161}Dy	5/2	0	0	79.6	25.7	^{163}Dy	5/2	137.9	250.9	0	0
$K = 5/2$	7/2	55.6	43.8	135.0	103.1	$K = 5/2$	7/2	204.8	285.6	67.4	73.4
$\omega = 0.923$	9/2	126.9	100.4	205.9	201.1	$\omega = 1.339$	9/2	290.5	336.5	153.7	167.3
$b = 0.599$	11/2	213.6	184.2	292.2	320.7	$b = 0.418$	11/2	394.8	412.4	258.7	281.6
$d_0 = 1000$	13/2	315.4	267.4	393.5	457.2	$d_0 = 1000$	13/2	517.3	497.2	382.1	415.2
$c = 2.57$	15/2	432.2	407.0			$c = 2.348$	15/2	657.7	627.7	523.4	568.7
RMS = 39	17/2	563.5	508.1			RMS = 48	17/2	682.5	734.3	815.7	740.0
	19/2	709.0	718.6				19/2	858.8	923.6	990.8	930.9
	21/2	868.4	826.1				21/2	1051.8	1046.8	1182.6	1137.1
	23/2	1041.2	1118.3				23/2	1261.2	1310.1	1390.7	1363.9
	25/2	1227.2	1221.8				25/2	1486.4	1431.0	1614.5	1601.3
							27/2	1727.0	1778.9	1853.6	1858.3
^{219}Fr	1/2	310.6		55.9	81.0	^{221}Fr	1/2	160.4	145.8	8.9	26.0
$K = 1/2$	3/2	229.6	210.4	153.1	139.8	$K = 1/2$	3/2	114.4	99.9	104.1	99.6
$\omega = 2.123$	5/2	390.7	384.3	17.4	15.0	$\omega = 0.138$	5/2	223.1	234.5	0	0
$b = 0.081$	7/2	201.8	191.3	244.1	269.2	$b = 0.29$	7/2	126.7	150.0	191.5	195.8
$d_0 = 6514$	9/2	491.5	506.5	0	0	$d_0 = 11$	9/2	300.5	294.8	44.5	38.5
$a = -11.28$	11/2	195.0	216.0	355.8	333.5	$a = -4.62$	11/2	170.9		286.0	
RMS = 17	13/2	419.4		199.5		RMS = 12	13/2	386.8		119.9	
^{223}Th						^{225}Th	3/2	0	0	13.4	
$K = 5/2$	5/2	0	0	36.5		$K = 1/2$	5/2	41.8	31	39.7	
$\omega = 0.446$	7/2	53.8	51.3	90.1		$\omega = 0.276$	7/2	78.7	68	98.1	
$b = 1.265$	9/2	122.5	118.9	158.5	180.5	$b = 5.7$	9/2	153.5	135	145.3	
$d_0 = 525$	11/2	205.7	212.3	241.3	243.0	$d_0 = 1159$	11/2	211.0	187	236.3	254
RMS = 14	13/2	303.0	320.0	338.2	324.1	$a = -0.226$	13/2	318.0	303	303.9	326
	15/2	448.6	428.7	413.8	412.4	RMS = 13	15/2	395.6	370	426.6	433
	17/2	572.0	569.6	537.7	547.3		17/2	533.8	530	513.9	520
	19/2	707.9	706.0	674.2	657.0		19/2	630.7	615	667.3	668
	21/2	855.8	858.1	822.6	838.1		21/2	799.0	807	773.5	769
	23/2	1015.0	1021.6	982.4	962.1		23/2	914.3	911	956.1	957
	25/2	1185.0	1185.4	1152.9	1179.4		25/2	1111.1	1127	1080.3	1072
	27/2	1365.1	1370.6	1333.7	1313.8		27/2	1243.9	1250	1290.6	1291
	29/2	1554.9	1551.7	1524.1	1558.4		29/2	1467.6	1485	1431.8	1426
	31/2	1753.7	1756.8	1723.6	1702.5		31/2	1617.0	1631	1668.3	1658
	33/2	1961.1	1952.7	1931.6			33/2	1866.0	1870	1825.4	1824
							35/2	2030.7	2047	2086.3	2057

TABLE III. The same as shown in Table II but for the nuclei ^{237}U and ^{239}Pu. Data from Ref. [19].

Nucl./K params.	I	$\pi=(+)$		$\pi=(-)$		Nucl./K params.	I	$\pi=(+)$		$\pi=(-)$	
		Th.	Exp.	Th.	Exp.			Th.	Exp.	Th.	Exp.
^{237}U	1/2	0	0	375.2		^{239}Pu	1/2	0	0	349.2	469.8
$K=1/2$	3/2	20.3	11.4	393.2		$K=1/2$	3/2	12.6	7.9	374.0	492.1
$\omega=1.46$	5/2	51.5	56.3	425.4		$\omega=1.58$	5/2	55.3	57.3	394.2	505.6
$b=0.102$	7/2	98.4	82.9	467.1		$b=0.107$	7/2	84.4	75.7	451.9	556.0
$d_0=618$	9/2	154.0	162.3	524.6		$d_0=791$	9/2	160.7	163.8	488.0	583.0
$a=0.038$	11/2	226.8	204.1	589.2		$a=-0.3$	11/2	206.0	193.5	577.7	661.2
RMS = 30	13/2	305.8	317.3	671.0		RMS = 63	13/2	314.8	318.5	629.1	698.7
	15/2	403.1	375.1	757.7	846.4		15/2	375.6	359.2	749.8	806.4
	17/2	504.2	518.2	862.4	930.0		17/2	515.4	519.5	816.0	857.5
	19/2	624.6	592.0	969.8	1027.5		19/2	590.9	570.9	966.0	992.5
	21/2	746.2	762.8	1096.1	1131.0		21/2	760.0	764.7	1046.2	1058.1
	23/2	888.0	853.0	1222.8	1250.7		23/2	849.4	828.0	1224.0	1219.4
	25/2	1028.5	1048.7	1369.1	1376.1		25/2	1045.9	1053.1	1317.3	1300.9
	27/2	1189.7	1155.1	1513.4	1515.7		27/2	1148.1	1127.8	1521.0	1487.4
	29/2	1347.5	1372.2	1678.0	1662.3		29/2	1369.9	1381.5	1626.4	1584.9
	31/2	1526.3	1494.1	1838.5	1821.8		31/2	1484.0	1467.8	1854.1	1795.4
	33/2	1699.7	1729.2	2019.8	1987.7		33/2	1729.1	1748.5	1970.7	1908.9
	35/2	1894.4	1868.2	2194.9	2166.5		35/2	1854.0	1847.0	2220.4	2143.4
	37/2	2081.7	2117.2	2391.2	2349.7		37/2	2120.3	2152.2	2347.4	2272.0
	39/2	2290.6	2272.2	2579.5	2547.5		39/2	2255.2	2263.0	2617.2	2529.4
	41/2	2490.5	2530.1	2789.3	2746.7		41/2	2540.7	2590.1	2753.6	2672.0
	43/2	2712.1	2702.5	2989.4	2960.5		43/2	2684.6	2714.0	3041.8	2951.4
	45/2	2922.9	2963.8	3211.2	3174.7		45/2	2987.6	3060.1	3186.7	3108.0
	47/2	3155.8	3154.5	3422.0	3401.5		47/2	3139.5	3198.0	3491.6	3407.0
	49/2	3376.5	3415.8	3654.6	3630		49/2	3458.3	3559.1	3644.2	3578.0
	51/2	3619.5	3625.5	3874.9	3865		51/2	3617.5	3713.0	3964.2	3895
	53/2	3848.9	3886.8	4117.1	4105		53/2	3950.5	4087.1	4123.8	4080.0
	55/2	4100.7	4115	4345.8	4344		55/2	4116.2	4256	4457.4	4413
	57/2	4338.0	4377	4596.7	4597						
	59/2	4597.7		4832.9	4835						

which is reasonably reproduced by the model. As shown below, the considerable number of experimental $B(E2)$ transition probabilities observed in both nuclei and several $B(E1)$ values available for ^{161}Dy allow a more detailed test of the model.

Also in Table II the results obtained for ^{219}Fr and ^{221}Fr illustrate the specific behavior of the model scheme in the case of a strong Coriolis interaction. We see that the level structures in ^{219}Fr with $I_0=(9/2)^-$ and $K=1/2$, and ^{221}Fr with $I_0=(5/2)^-$ and $K=1/2$, are strongly perturbed, with quite large values $a=-11.28$ and $a=-4.02$, respectively, obtained for the Coriolis decoupling parameter. In the two nuclei several states with lower angular momenta appear at higher energy with respect to their neighbors. In such a way the ground states of both nuclei appear with higher angular momenta with respect to several higher-energy states. This complicated structure of the spectrum is reproduced within the model scheme due to the Coriolis term in the model Hamiltonian.

Again in Table II, the good model description of the split-parity doublet structure in the nuclei ^{223}Th and ^{225}Th is demonstrated. We remark that these nuclei represent the odd-A counterparts of the respective even-even thorium nuclei providing the best examples for nuclear quadrupole-octupole collectivity. In Table III the result for the longer level sequences in ^{237}U and ^{239}Pu is illustrated. This result suggests that the parity doublet structure of the spectrum can be developed to rather high angular momenta such as $I=59/2$ with the model scheme being still capable of reproducing it.

The obtained numerical results allow an analysis of the parity doublet splitting, given by the quantity $\Delta E(I^{\pm})=E(I^+)-E(I^-)$, as a function of the angular momentum. This quantity is sensitive to the Coriolis interaction and exhibits a staggering behavior indicating the respective perturbation of the spectrum. In Fig. 1 it is illustrated that the model calculations reproduce the staggering behavior of $\Delta E(I^{\pm})$ induced by the Coriolis interaction in the spectra of ^{219,221}Fr, ^{219,225}Ra, ^{219}Ac, and ^{225}Th with $K=1/2$. In Fig. 2 we observe a smooth behavior of $\Delta E(I^{\pm})$ as a function of I for the nuclei ^{225}Fr, ^{225}Ac, ^{231}Th, ^{239,243}Am, and ^{245}Cm where $K\neq 1/2$ and the Coriolis effect does not perturb the spectrum. The near linear dependence of the doublet splitting, is clearly explained through the decrease of the ratio $k^2/I(I+1)$ with the increasing angular momentum in Eq. (13). As explained in the end of Sec. III, this behavior can be associated with the forming of a degenerate parity doublet structure at higher angular momenta and has a clear physical meaning.

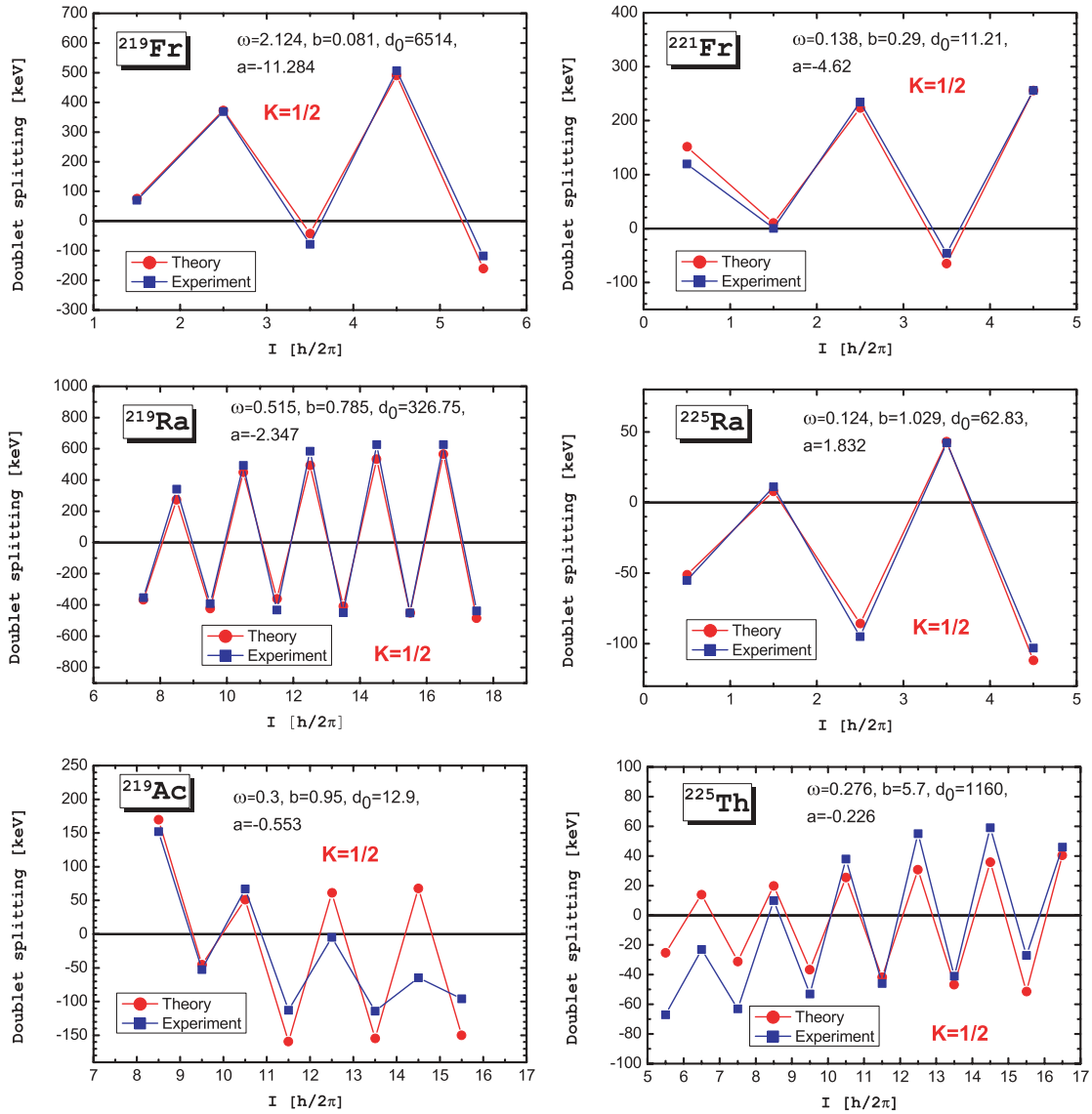

FIG. 1. (Color online) Experimental and theoretical parity-doublet splitting in ^{219,221}Fr, ^{219,225}Ra, ^{219}Ac, and ^{225}Th. The data for ^{221}Fr and ^{225}Th are taken from Refs. [17] and [18], respectively, whereas those for the other nuclei are from Ref. [16].

The above analysis allows a detailed estimation of the possible values of the angular momentum projection K on which the parity-doublet structure is built. This is illustrated in Fig. 3 through the doublet splitting $\Delta E(I^{\pm}) = E(I^{+}) - E(I^{-})$ observed in ^{223}Ra. It is seen in Fig. 3(a) that the experimentally assumed value $K = 3/2$ does not support the staggering behavior of the parity splitting observed in the experimental data. Figure 3(b) shows that if a $K = 1/2$ value is assumed, the staggering behavior of $\Delta E(I^{\pm})$ is reproduced. In such a way the presence of the staggering effect indicates a strong contribution of an intrinsic $K = 1/2$ configuration related to the Coriolis coupling interaction. The considered example suggests a possibility to get information about the single-particle orbitals that contribute to the K configurations associated with the particular collective spectrum of the nucleus.

We have implemented model calculations for $B(E2)$ and $B(E1)$ reduced transition probabilities in the spectra of ^{161,163}Dy, ^{151}Pm, ^{227}Ra, and ^{239}Np, where the available experimental data allow to get information about the angular momentum dependence of these quantities. The theoretical transition values have been determined after fitting the parameter c in Eqs. (22) and (23). The scaling (effective charge) parameters were taken as $b_2 = 10^3$ in all nuclei and $b_1 = 2 \times 10^{-4}$ for ^{161}Dy and $b_1 = 10^{-4}$ for the remaining nuclei. The calculated results are compared to experimental data in Figs. 4–8. Figure 4 shows the behavior of $B(E1)$ transition probabilities between positive- and negative-parity counterparts in the spectrum of ^{161}Dy. The data, which are reasonably reproduced by the theoretical values, indicate a decrease of this quantity with increasing angular momentum. Although the number of experimental points is not enough to draw a detailed conclusion, the observed behavior of $B(E1)$

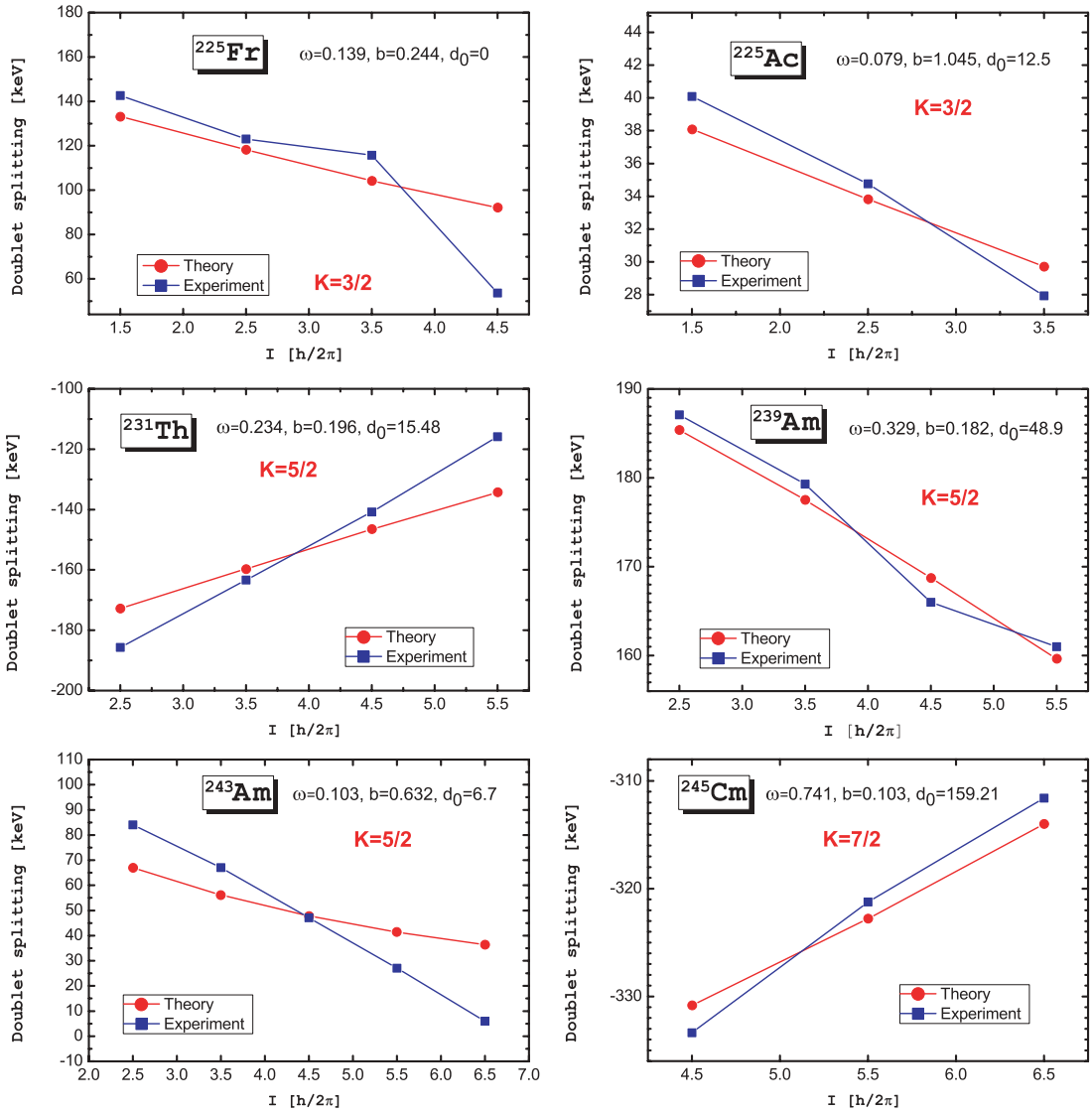

FIG. 2. (Color online) The same as in Fig. 1 but for the nuclei ^{225}Fr, ^{225}Ac, ^{231}Th, ^{239,243}Am, and ^{245}Cm. Data from Ref. [15].

can be interpreted within the model framework. Based on the remark in the end of Sec. III, the decreasing model values of $B(E1)$ can be associated with the respective decrease in the doublet splitting. In the limiting case of degeneracy this transition probability is completely reduced. Considering that toward the degeneracy limit the collective dynamics of the nucleus is less affected by the single-particle parity, one can suppose that the quenched $B(E1)$ transition probabilities between positive- and negative-parity counterparts at higher angular momenta are no longer of a prominent collective character.

In Figs. 5 and 6 the results for the $B(E2)$ transition probabilities within sequences of a given parity of the nuclei ^{161}Dy and ^{163}Dy are shown. We see that the theory reproduces the overall behavior of the experimental data in the cases of $\Delta I = 1$ and $\Delta I = 2$ transitions. Some staggering behavior of $B(E2)$ is observed in the data of ^{161}Dy. As far as the $E2$ transitions are of quadrupole character one may suppose that such perturbations in the $B(E2)$ values are due to the mixing with other level sequences in the spectrum based on quadrupole degrees of freedom [16]. However, the integral (23) incorporates the simultaneous contribution of the quadrupole and octupole degrees of freedom in the level energies. Therefore the $B(E2)$ transition values between members of the parity doublet also carry the sign of quadrupole-octupole collectivity.

Figs. 7 and 8 show some additional results for $B(E1)$ transition probabilities between positive- and negative-parity states in ^{151}Pm, ^{227}Ra, and ^{239}Np. In all cases there are more than enough data to draw detailed conclusions. Nevertheless, we can point out that the indication for decrease in the $B(E1; I^{\pi} \to I^{-\pi})$ values in these nuclei, Fig. 7 and Fig. 8(a), supports the above interpretation made for ^{161}Dy (Fig. 4). In the case of the $B[E1; I^{-} \to (I+1)^{+}]$ transitions in ^{227}Ra, Fig. 8(b), both experiment and theory give an indication for an increase with angular momentum. All these results suggest that

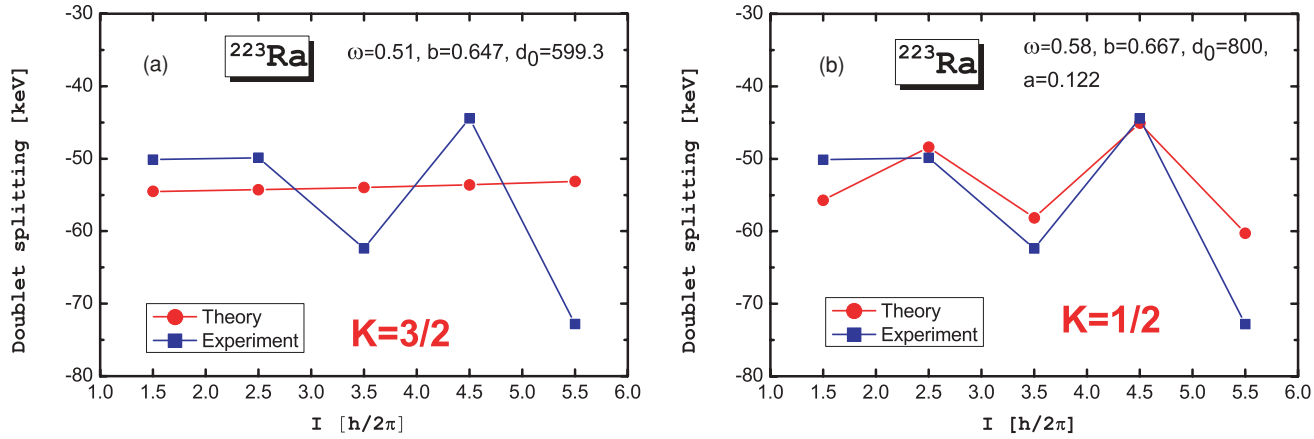

FIG. 3. (Color online) Experimental and theoretical doublet splitting in ^{223}Ra with (a) $K = 3/2$ and (b) $K = 1/2$. Data from Ref. [16].

any further experimental data would provide important information about the angular momentum evolution of quadrupole-octupole collectivity in the split-parity doublet spectra.

We have examined the way in which the model formalism can be limited to the presence of the quadrupole collective mode alone, without explicitly breaking the assumption for the coherence between quadrupole and octupole degrees of freedom. In this limit the reduced contribution of the octupole mode is related to the gradual reduction of the interaction between positive- and negative-parity counterparts of the split-parity doublet. The model quantity related to the magnitude of this interaction is the difference $\Delta k^2 = |k_+^2 - k_-^2|$ in the quantum number k, which separates energetically the counterparts according to Eq. (13) [see also the text below Eqs. (15) and (16)]. In the present work Δk^2 is taken equal to 3, providing a relatively weak splitting of the parity doublet that corresponds to a considerable presence of the octupole degree of freedom. With the increasing Δk^2 the doublet splitting increases and the octupole interaction between the opposite-parity counterparts, respectively, decreases. In the limiting case

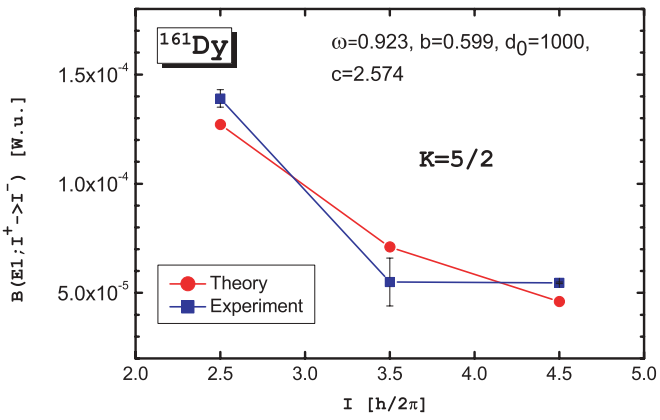

FIG. 4. (Color online) Theoretical and experimental $B(E1)$ transition probabilities between positive- and negative-parity counterparts in the spectrum of ^{161}Dy. Data from Ref. [15]. The $B(E1)$ values are quite similar in the case of separately fitted positive- and negative-parity bands with the same $k_{\text{fix}} = 1$. See Table V for comparisons.

of large enough Δk^2 ($\Delta k^2 \to \infty$) the doublet is completely split. Then both, the positive- and negative-parity sequences are completely separated and do not interact to each other, a situation opposite to the degeneracy limit. As a result there is no manifestation of octupole degree of freedom. This situation is reproduced by the model formalism as follows. The energy sequence containing the ground state is characterized by the lowest value of k, $k_0 = 1$ or 2, depending on the ground-state parity, (+) or (−), respectively. The opposite-parity levels are characterized by a large $k \gg k_0$ value, which shifts them up to a different (higher) energy range. In such a way only the ground-state energy sequence remains in the model framework and it is associated to the quadrupole degrees of freedom only. As a main consequence of reduced octupole interaction, the $B(E1)$ transition probabilities between states with positive and negative parity become zero. At the same time the $B(E2)$ transition probabilities within the ground-state energy sequence correspond to pure quadrupole rotations and vibrations. However, because the $E2$ transitions are of quadrupole character and the octuple mode affects them only indirectly, as mentioned above, one should not expect considerable change in the $B(E2)$ values toward the quadrupole limit. Note that in this limit the quadrupole-octupole model describing two coupled energy sequences with opposite parities is reduced to a simple quadrupole model for one band with fixed parity.

The above discussed quadrupole limit of the model can also be derived by directly removing the octupole variable from the model Hamiltonian (1), i.e., by taking $C_3 = 0$ and $d_3 = 0$ in the potential (4) and solving the one-dimensional Schrödinger equation for β_2 in a potential of Davidson's type. However, the present analysis shows how this limit can be gradually obtained through the increase of the model quantity Δk^2, which has a clear physical meaning related to the magnitude of the octupole interaction. We remark that a similar mechanism of complete multiplet splitting with reduced interband interaction is known for the ground and γ bands of even-even nuclei within the concept of broken SU(3) symmetry [20].

We examined the behavior of theoretical $B(E1)$ and $B(E2)$ transition probabilities for ^{161}Dy and ^{163}Dy in the above

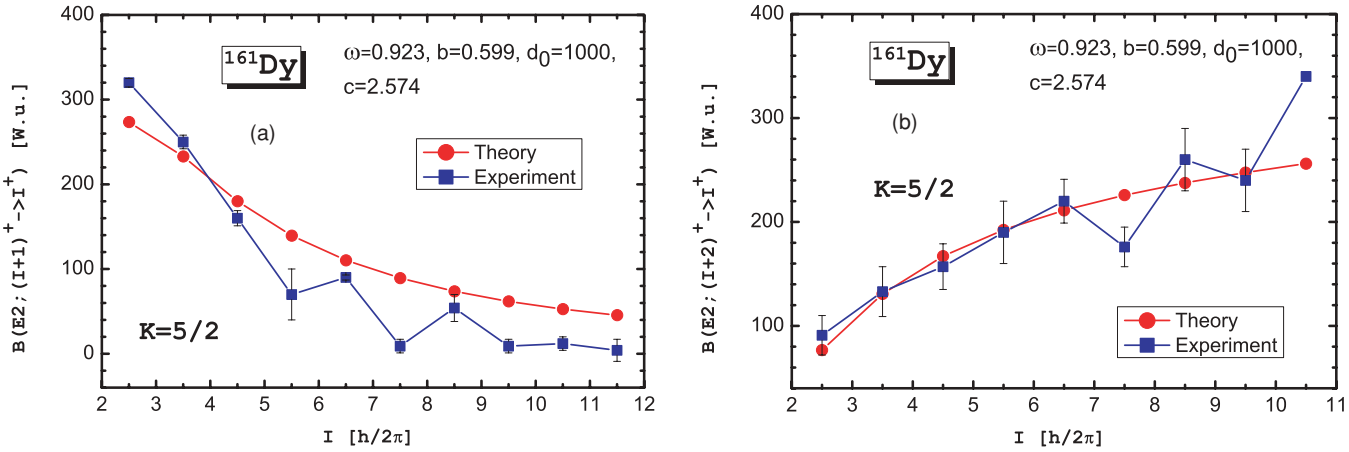

FIG. 5. (Color online) Theoretical and experimental $B(E2)$ transition probabilities in the positive-parity sequence of ^{161}Dy with: (a) $\Delta I = 1$, (b) $\Delta I = 2$. Data from Ref. [15]. The $B(E2)$ values are almost identical in the pure quadrupole limit. See Table IV for the comparison.

considered limit of completely split-parity doublet. For this purpose the ground-state sequences of both nuclei were associated with $k_+ = 1$ (for $\pi = +$) and $k_- = 2$ (for $\pi = -$), respectively. The corresponding opposite-parity counterparts were associated with the large values $k_- = 30$ (for ^{161}Dy) and $k_+ = 31$ (for ^{163}Dy). The model calculations have been implemented only for the ground state sequences by keeping in the $B(E1)$ and $B(E2)$ transitions the same values of the effective charge parameters as in the complete quadrupole-octupole case. As a result we verified that the theoretical $B(E1)$ transition values between the $(5/2)^{\pm}$, $(7/2)^{\pm}$, and $(9/2)^{\pm}$ parity counterparts in ^{161}Dy, shown in Fig. 4 for the quadrupole-octupole case now drop to zero. In this meaning the nonzero experimental values for these transitions, together with their reasonable model description in Fig. 4 indicate the presence of coherent quadrupole-octupole modes in the spectrum of ^{163}Dy. The above conclusion holds also for the $B(E1)$ transition values in Figs. 7 and 8.

The results for the $B(E2)$ transition probabilities within the ground-state sequences of ^{161}Dy and ^{163}Dy obtained in the quadrupole-octupole framework and in the quadrupole limit of the model are given in Table IV together with the respective

TABLE IV. Theoretical and experimental $B(E2)$ values (in W.u.) in the ground-state sequences of ^{161}Dy (with positive parity) and ^{163}Dy (with negative parity). The column Qoc. corresponds to model calculations with quadrupole and octupole modes, while the column Quad. corresponds to calculations in the quadrupole limit. See the text for more details.

$I_i \to I_f$	^{161}Dy $(\pi = +)$		Exp.	^{163}Dy $(\pi = -)$		Exp.
	Qoc.	Quad.		Qoc.	Quad.	
$7/2 \to 5/2$	273	269	320 (5)	304	309	281 (14)
$9/2 \to 7/2$	233	229	250 (8)	259	263	260 (60)
$11/2 \to 9/2$	180	178	160 (9)	200	202	–
$13/2 \to 11/2$	140	139	70 (30)	155	156	200 (80)
$15/2 \to 13/2$	110	110	90 (3)	123	123	120 (30)
$17/2 \to 15/2$	89	89	9 (8)	100	99	36 (9)
$19/2 \to 17/2$	74	74	54 (16)	82	81	44 (16)
$21/2 \to 19/2$	62	63	9 (8)			
$23/2 \to 21/2$	53	54	12 (8)			
$25/2 \to 23/2$	45	47	4 (9, −4)			
$9/2 \to 5/2$	77	75	91 (19)	85	87	110 (20)
$11/2 \to 7/2$	131	129	133 (24)	145	147	–
$13/2 \to 9/2$	167	165	157 (22)	186	188	200 (80)
$15/2 \to 11/2$	192	192	190 (30)	214	215	292 (70)
$17/2 \to 13/2$	211	211	220 (21)	236	235	250 (40)
$19/2 \to 15/2$	226	227	176 (19)	252	250	260 (4)
$21/2 \to 17/2$	238	240	260 (30)	266	262	250 (43)
$23/2 \to 19/2$	248	252	240 (30)	277	271	230 (50)
$25/2 \to 21/2$	256	262	340 (7)			

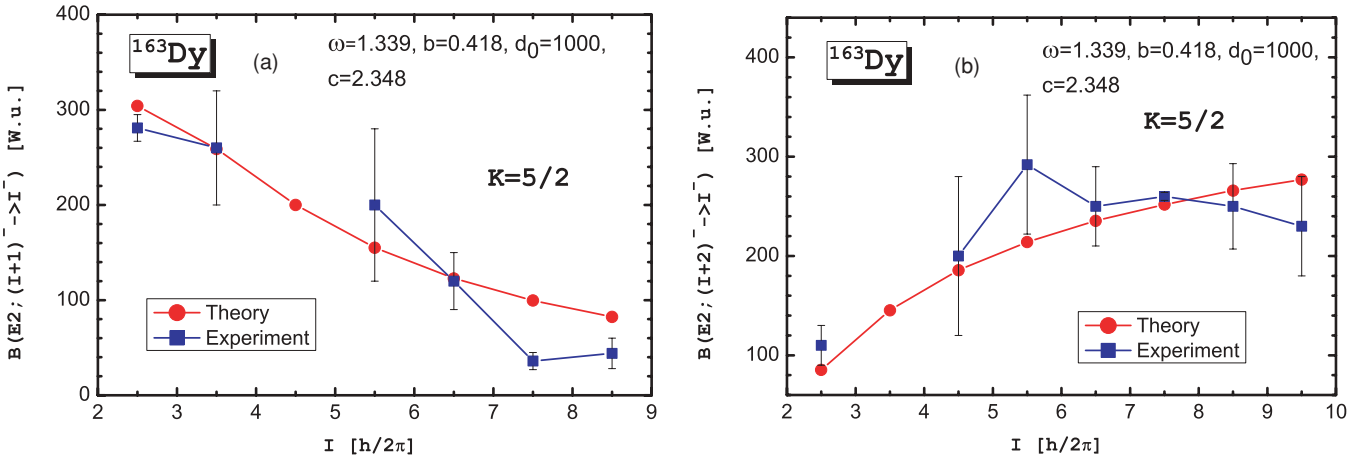

FIG. 6. (Color online) The same as in Fig. 5, but for the negative-parity sequence of ^{163}Dy. Data from Ref. [15].

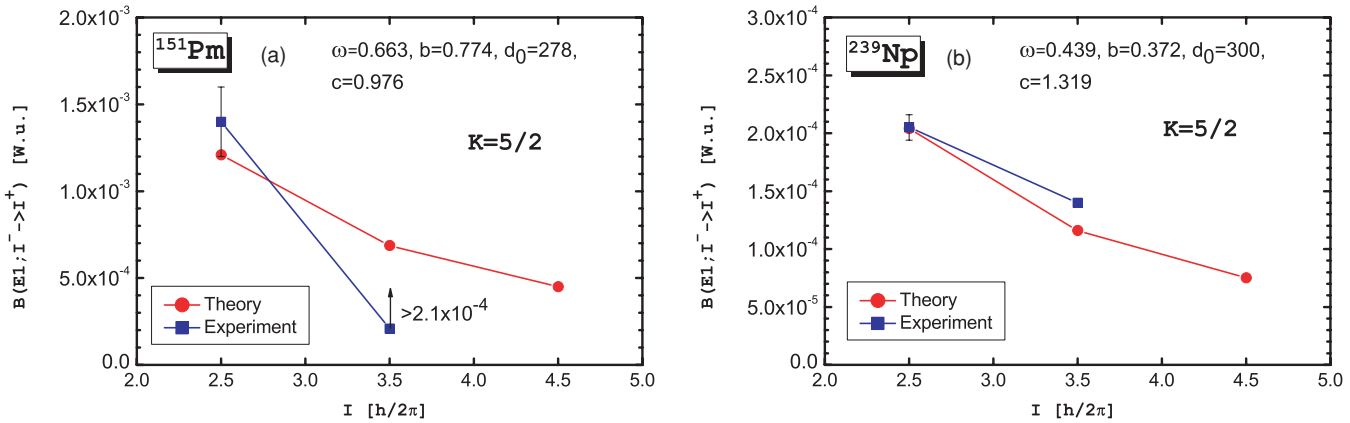

FIG. 7. (Color online) Theoretical and experimental $B(E1)$ transition probabilities between negative- and positive-parity counterparts in the spectra of ^{151}Pm and ^{239}Np. Data from Ref. [15].

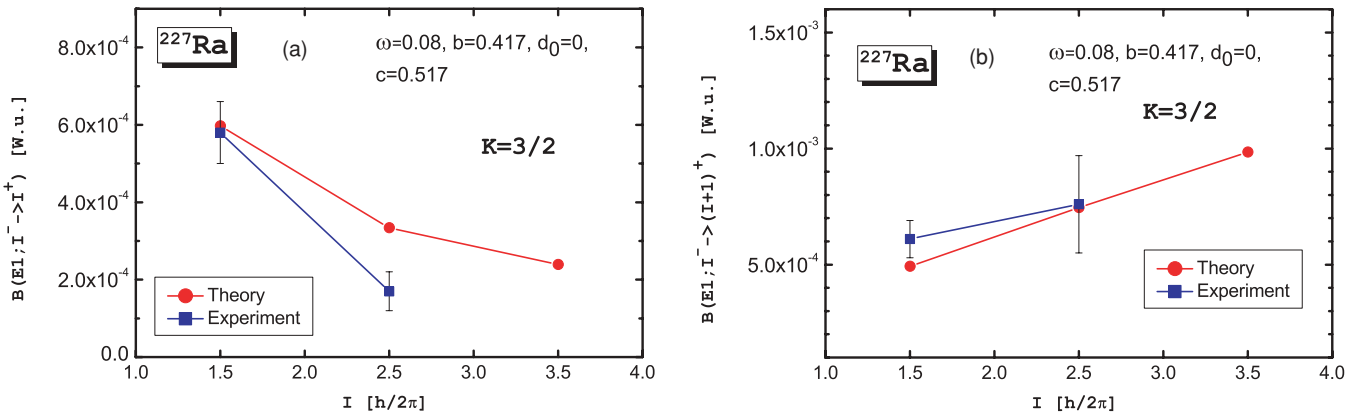

FIG. 8. (Color online) Theoretical and experimental $B(E1)$ transition probabilities between (a) negative- and positive-parity counterparts and (b) negative- and positive-parity states with $\Delta I = 1$ in the spectra of ^{227}Ra. Data from Ref. [15].

TABLE V. Theoretical and experimental $B(E1)$ values (in W.u.) for $E1$ transitions between negative- and positive-parity states in ^{151}Pm, ^{161}Dy, ^{227}Ra, and ^{239}Np (data from [15]). The column Qoc corresponds to model calculations with quadrupole and octupole modes, whereas the column k_{fix} corresponds to calculations with the same value of the model quantum number $k = 1$ for the positive- and negative-parity states. The parameters units are the same as in Table II. See the text for more details.

Nucl.	Separate bands params. for k_{fix}			$E1$ transitions	$B(E1)$ transition values		
	Param.	Band (+)	Band (−)	$I_i \to I_f$	Qoc	k_{fix}	Exp.
^{151}Pm	ω	0.107	0.091	$5/2^- \to 5/2^+$	0.001208	0.001488	0.0014 (2)
	b	30.1	30.1	$7/2^- \to 7/2^+$	0.000686	0.000451	>0.000210
	d_0	270	270				
	c	2.2	2.2				
^{161}Dy	ω	1.052	1.388	$5/2^- \to 5/2^+$	0.000127	0.000107	0.000139 (4)
	b	0.5	0.5	$7/2^- \to 7/2^+$	0.000071	0.000060	0.000055 (11)
	d_0	1000	1000	$9/2^- \to 9/2^+$	0.000046	0.000039	0.000054 (4)
	c	2.57	2.57				
^{227}Ra	ω	0.627	0.107	$3/2^- \to 3/2^+$	0.000597	0.000624	0.00058 (8)
	b	0.42	0.41	$3/2^- \to 5/2^+$	0.000493	0.000412	0.00061 (8)
	d_0	600	100	$5/2^- \to 5/2^+$	0.000334	0.000282	0.00017 (5)
	c	0.7	0.7	$5/2^- \to 7/2^+$	0.000746	0.000516	0.00076 (21)
^{239}Np	ω	0.376	0.510	$5/2^- \to 5/2^+$	0.000204	0.000212	0.000205 (11)
	b	0.37	0.37	$7/2^- \to 7/2^+$	0.000116	0.000120	>0.000140
	d_0	300	300				
	c	1.3	1.3				

experimental data. It is seen that the $B(E2)$ values are almost identical in the pure quadrupole limit. See Table IV for the comparison. Thus, the exclusion of the octupole degree of freedom in the quadrupole limit does not affect considerably the behavior of these transition values. The comparison of both theoretical sets of data in Table IV illustrates the slight indirect influence of the octupole degree of freedom on the quadrupole-defined $B(E2)$ transitions.

We remark that non-zero $B(E1)$ transition values can be obtained by taking the same fixed value $k_{\text{fix}} = k_+ = k_- = 1$ of the model quantum number k in Eq. (13) and separate (independent) sets of parameters ω, b, and d_0 for the both, positive- and negative-parity sequences. (Only the parameter c related through multiplication to the effective charge should be kept the same for both sequences.) Results of such a calculation for ^{151}Pm, ^{161}Dy, ^{227}Ra, and ^{239}Np are shown in Table V. We see that the obtained $B(E1)$ values are close to those obtained in the coherent quadrupole-octupole calculation. However, one should keep in mind that if the model quantum number k is the same for both sequences it does not take into account anymore the difference in the parity of the counterpart states. Then the parity of the states should be assumed beyond the considered formalism.

Finally, it is worth noting that our analysis outlines two limits in the coherent quadrupole-octupole motion of the system. First, this is the limit of doublet degeneracy realized for a finite value of Δk^2 (as $\Delta k^2 = 3$) and increasing angular momentum. Second, the limit of completely split-parity doublet is realized at large values of Δk^2. Note that in the first case the reduction of the $B(E1)$ transition values with the angular momentum is associated with degeneracy, whereas in the second case the missing $B(E1)$ transitions mean no presence of octupole mode in the collective motion of the system. The systematic behavior of nuclear quadrupole-octupole collectivity with respect to these limits is a subject of further work.

VI. CONCLUSIONS

In conclusion, the model scheme based on coherent quadrupole-octupole oscillations and rotations with a Coriolis coupling to a single particle suggests a collective mechanism for the appearance of split-parity doublet structures in odd-A nuclei. The model reproduces split-parity doublet spectra in a wide range of nuclei with a good accuracy and provides predictions for further not yet observed energy levels. It describes the fine staggering behavior of the doublet-splitting as a function of the angular momentum. In this framework the Coriolis interaction has important influence on the structure of the split-parity doublets. The formalism provides respective estimations for the possible values of the angular momentum projection K on which the spectrum is built. Thus, one can get information about the intrinsic K configurations associated with the collective energy bands of odd-A nuclei. The analysis of $B(E1)$ and $B(E2)$ transition probabilities in the split parity-doublet spectra outlines the relation between the different states within the spectrum. The particular behavior of the doublet splitting and the $B(E1)$ values between opposite-parity counterparts in dependence on the angular momentum suggests the way in which a degenerate doublet structure can be formed. The limit of missing octupole mode is associated with the situation of completely split (disintegrated) parity doublet structure. Finally, the present model approach gives a physical framework for the evolution of quadrupole-octupole collectivity in odd-A nuclei and outlines the limits of its manifestation in the different nuclear regions.

ACKNOWLEDGMENTS

We thank Professor R. V. Jolos for valuable discussions and comments. This work is supported by DFG and by the Bulgarian Scientific Fund (BSF) under contract F-1502/05. One of the authors (S.L.) acknowledges the support by BSF contract MU-405/05.

[1] A. Bohr and B. R. Mottelson, *Nuclear Structure* (Benjamin, New York, 1975), Vol. II.
[2] P. A. Butler and W. Nazarewicz, Rev. Mod. Phys. **68**, 349 (1996).
[3] H. J. Krappe and U. Wille, Nucl. Phys. **A124**, 641 (1969).
[4] G. A. Leander, R. K. Sheline, P. Möller, P. Olanders, I. Ragnarsson, and A. J. Sierk, Nucl. Phys. **A388**, 452 (1982).
[5] R. Jolos, P. von Brentano, and F. Dönau, J. Phys. G **19**, L151 (1993).
[6] R. V. Jolos, and P. von Brentano, Phys. Rev. C **49**, R2301 (1994).
[7] A. Ya. Dzyublik and V. Yu. Denisov, Yad. Fiz. **56**, 30 (1993) [Phys. At. Nucl. **56**, 303 (1993)].
[8] V. Yu. Denisov and A. Ya. Dzyublik, Nucl. Phys. **A589**, 17 (1995).
[9] N. Minkov, P. Yotov, S. Drenska, W. Scheid, D. Bonatsos, D. Lenis, and D. Petrellis, Phys. Rev. C **73**, 044315 (2006).
[10] J. P. Davidson, *Collective Models of the Nucleus* (Academic Press, New York, 1968).
[11] P. M. Davidson, Proc. R. Soc. London Ser. A **135**, 459 (1932).
[12] J. P. Elliott, J. A. Evans, and P. Park, Phys. Lett. **B169**, 309 (1986).
[13] D. J. Rowe and C. Bahri, J. Phys. A **31**, 4947 (1998).
[14] R. V. Jolos, N. Minkov, and W. Scheid, Phys. Rev. C **72**, 064312 (2005).
[15] http://www.nndc.bnl.gov/ensdf/, as of March 2007.
[16] A. Jungclaus, B. Binder, A. Dietrich, T. Härtlein, H. Bauer, Ch. Gund, D. Pansegrau, D. Schwalm, D. Bazzacco, E. Farnea, S. Lunardi, C. Rossi-Alvarez, C. Ur, G. de Angelis, A. Gadea, D. R. Napoli, X. R. Zhou, and Y. Sun, Phys. Rev. C **67**, 034302 (2003).
[17] R. K. Sheline, Phys. Lett. **B205**, 11 (1988).
[18] J. R. Hughes, R. Tölle, J. De Boer, P. A. Butler, C. Günther, V. Grafen, N. Gollwitzer, V. E. Holliday, G. D. Jones, C. Lauterbach, M. Marten-Tölle, S. M. Mullins, R. J. Poynter, R. S. Simon, N. Singh, R. J. Tanner, R. Wadsworth, D. L. Watson, and C. A. White, Nucl. Phys. **A512**, 275 (1990).
[19] S. Zhu, R. V. F. Janssens, G. J. Lane, I. Wiedenhöver, M. P. Carpenter, I. Ahmad, A. P. Byrne, P. Chowdhury, D. Cline, A. N. Deacon, G. D. Dracoulis, S. J. Freeman, N. J. Hammond, G. D. Jones, T. L. Khoo, F. G. Kondev, T. Lauritsen, C. J. Lister, A. O. Macchiavelli, E. F. Moore, D. Seweryniak, J. F. Smith, and C. Y. Wu, Phys. Lett. **B618**, 51 (2005).
[20] N. Minkov, S. B. Drenska, P. Raychev, R. Roussev, and D. Bonatsos, Phys. Rev. C **60**, 034305 (1999).